The FEBS Journal

FEBS PRESS science publishing by scientists

Structural insight into the Scribble PDZ domains interaction with the oncogenic Human T-cell lymphotrophic virus-1 (HTLV-1) Tax1 PBM

Airah Javorsky[1], Janesha C. Maddumage[1], Emily R. R. Mackie[1], Tatiana P. Soares da Costa[1], Patrick O. Humbert[1,2,3,4] and Marc Kvansakul[1,2]

1 Department of Biochemistry & Chemistry, La Trobe Institute for Molecular Science, La Trobe University, Melbourne, Vic., Australia
2 Research Centre for Molecular Cancer Prevention, La Trobe University, Melbourne, Vic., Australia
3 Department of Biochemistry & Pharmacology, University of Melbourne, Melbourne, Vic., Australia
4 Department of Clinical Pathology, University of Melbourne, Melbourne, Vic., Australia

Keywords
cell polarity; HTLV-1; human T lymphotrophic virus-1; isothermal titration calorimetry; PDZ; scribble; Tax1; X-ray crystallography

Correspondence
M. Kvansakul and P. O. Humbert, Department of Biochemistry & Chemistry, La Trobe University, Melbourne, Vic. 3086, Australia
Tel: +61 3 9479 2263 (M.K.); +61 3 9479 5155 (P.O.H.)
E-mail: m.kvansakul@latrobe.edu.au (M.K.); p.humbert@latrobe.edu.au (P.O.H.)

(Received 27 January 2022, revised 14 July 2022, accepted 25 August 2022)

doi:10.1111/febs.16607

Scribble (Scrib) is a highly conserved cell polarity regulator that harbours potent tumour suppressor activity and plays an important role in cell migration. Dysregulation of polarity is associated with poor prognosis during viral infections. Human T-cell lymphotrophic virus-1 (HTLV-1) encodes for the oncogenic Tax1 protein, a modulator of the transcription of viral and human proteins that can cause cell cycle dysregulation as well as a loss of genomic integrity. Previous studies established that Scribble interacts with Tax1 via its C-terminal PDZ-binding motif (PBM), leading to aggregation of polarity regulators and subsequent perturbation of host cell adhesion, proliferation, and signalling. Using isothermal titration calorimetry, we now show that all four PDZ domains of Scribble bind to Tax1 PBM. We then determined crystal structures of Scribble PDZ1, PDZ2 and PDZ3 domains bound to Tax1 PBM. Our findings establish a structural basis for Tax1-mediated subversion of Scribble-mediated cell polarity signalling and provide the platform for mechanistic studies to examine Tax1 induced mislocalization of Scribble and the associated changes in cellular architecture and subsequent tumorigenesis.

Introduction

Cell polarity refers to the differential distribution of cellular macromolecules, which is essential for normal development and function [1–3] and allows for the appropriate orientation of a cell. Loss of cell polarity leads to tissue disorganization and excessive cell proliferation, both of which are associated with tumorigenesis or viral replication [4]. Cell polarity can be divided into four general forms: apico-basal cell polarity, planar cell polarity, asymmetric cell division, and front-rear cell polarity. In addition, a number of specialized forms of cell polarity have been described for specific cell types including T-cell immunological synapse formation, neuronal axon specification and myelin sheet formation in oligodendrocytes [3,5–7]. Three major evolutionary conserved protein modules are generally involved in an antagonistic relationship to establish cell polarity in many of these systems; the PAR complex, Crumbs complex and the Scribble complex [2,8]. The Scribble module comprises three proteins, Scrib, Dlg, and Lgl, which are all adaptor proteins featuring multiple protein interaction domains that allow engagement of a host of cellular interactors to regulate

Abbreviations
ATL, adult T-cell leukaemia; AUC, analytical ultracentrifugation; ITC, isothermal titration calorimetry; LAPSD, LAP-specific domains; LRRs, leucine-rich repeats; PBM, PDZ-binding motif; PLA, proximity ligation; Scrib, Scribble.

cell signalling, however, their function is also dependent on their cellular localization [2].

The human Scribble protein (SCRIB) is 1630 residues long and a member of the LAP (leucine-rich repeats and PDZ domain) protein family, and comprises 16 LRRs (Leucine-rich repeats), two LAP-specific domains (LAPSDa and LAPSDb) and the four PDZ domains (PDZ1, PDZ2, PDZ3, and PDZ4) (Fig. 1A) [9]. In particular, the PDZ domains have been shown to be the mediators for the vast majority of Scribble interactions with ligands, with the LRR domain playing less of a role for interactions and

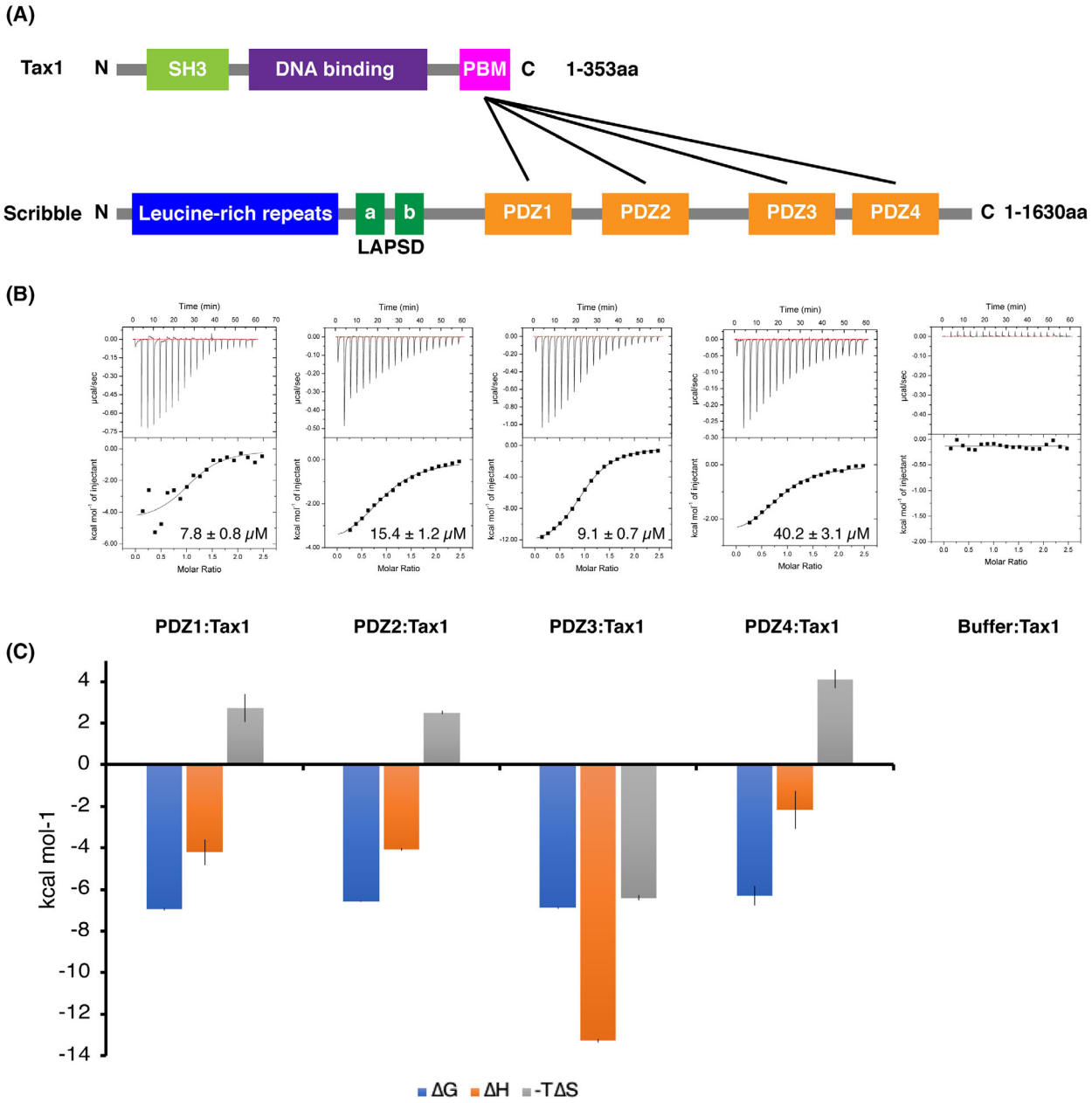

Fig. 1. (A) schematic outline of HTLV-1 Tax1 and Scribble interaction. Black line indicating the domains of interaction. (B) Interaction profiles of SCRIB PDZ domains with the Tax1 PBM peptide. Thermograms showing heat of titrations from isothermal titration calorimetry. K_D values (in μM) are the means of 3 experiments ± SD. (C) Thermodynamic analysis of the interactions between SCRIB PDZ domains and Tax1 PBM shown as the means of 3 experiments ± SD. The contribution of $-\Delta H$ (kcal·mol^{-1}) and $T\Delta S$ (kcal·mol^{-1}·K^{-1}) to the binding of Tax1 peptide are shown.

primarily impacting correct localization of the Scribble module within the cytoplasm [2,10]. PDZ domains are typically ~ 90 residues in size and consist of 5 to 6 β-strands and 2 to 3 α-helices, which allow for the formation of a conserved binding groove between the second α-helix and the second β-strand [11]. This structure allows PDZ domains to recognize short amino acid sequences coined PDZ-binding motifs (PBMs) at the extreme C-termini of interacting proteins, however several PDZ domains have now also been shown to recognize internal PBM sequences [2,12].

Scribble is vital for T-cell maturation and division and is localized with Dlg in T-cell antigen presentation and the uropod, a single protrusion formed during cell–cell interactions and migration [8,13,14]. Several viruses have been shown to encode interactors of Scribble, including Influenza A NS1, TBEV NS5, and HPV-18 E6 as well as HTVL-1 encoded *Tax1* [15–20]. HTLV-1 is single-stranded RNA T-lymphotropic tumour virus and the etiological pathogen of several human diseases, including adult T-cell leukaemia (ATL), HTLV-1-associated myelopathy/tropical spastic paraparesis, and inflammatory disorders such as uveitis and dermatitis [21,22]. The virus spreads primarily via cell-to-cell transmission, induces clonal proliferation of infected T cells *in vivo*, and after a long latency period, a subset of HTLV-1 carriers develop ATL [23]. HTLV-1 is a direct cause of ATL and is dependent on the expression of the oncogenic protein Tax1 for the maintenance of the malignancy [24]. Tax exists in two forms, Tax1 and Tax2 which correlate to their parent viruses HTLV-1 and HTLV-2, respectively [25]. They share high sequence homology but differ at the structural and functional level [25]. Both Tax1 and 2 harbour multiple activities including the ability to transcriptionally activate cellular genes through NF-kB, CREB/ATF, SRF, and AP-1 and the inactivation of tumour suppressor proteins p53 and p16INK4a [26–29]. However Tax1 and Tax2 differ significantly in their transforming activities *in vitro* [30]. For instance, Tax1 transforms a mouse T-cell line CTLL-2 from interleukin (IL)-2-dependent growth into independent growth with substantially greater efficiency compared with Tax2 [25,30,31]. Subsequently it was shown that this difference is due to the presence of a C-terminal PBM in Tax1, and Tax1-mediated activation of the transcription factor NF-kB [32].

Tax1 PBM binds to numerous polarity proteins and leads to the aggregation or mislocalization of Dlg, Scribble, MAGI-1 and MAGI-3 [33–36], impacting host cell control of cell adhesion, proliferation, and signalling. In humanized CD34+ mice, Tax1 PBM enhances HTLV-1-induced T-cell proliferation [33]. Immunofluorescence (IF) and *in situ* proximity ligation (PLA) assays revealed that Tax1 and Scribble co-localized as large granules near the cell membrane. In contrast, such aggregates were not detected in a Tax1 mutant lacking the PBM motif, suggesting that the ability of Tax1 to sequester Scribble is PBM dependent [33].

We now report the systematic examination of the Tax1 C-terminal PBM interactions with human Scribble PDZ domains using isothermal titration calorimetry, which revealed that all four Scribble PDZ domains are Tax1 interactors. Furthermore, we determined crystal structures of Scribble PDZ1, 2, and 3 domains bound to the Tax1 PBM. Our findings provide a structural basis for Tax1-mediated subversion of Scribble polarity signalling.

Results

Interactions of SCRIB PDZ domains with Tax1 PBM

To understand the impact of Tax1 binding to Scribble on polarity signalling, we examined the affinity of recombinant human Scribble (SCRIB) PDZ1, 2, 3, and 4 domains for an 8-mer peptide encoding for the Tax1 PBM (Fig. 1B,C). Unexpectedly, our isothermal titration calorimetry (ITC) measurements revealed that Tax1 bound to all Scribble PDZ domains with an affinity of 7.8 μM for PDZ1, 15.4 μM for PDZ2, 9.1 with PDZ3, and 40.2 with PDZ4 (Table 1). Examination of the thermodynamic-binding parameters of Tax1 binding to Scribble PDZ domains revealed that binding is largely entropy-driven by a more favourable $-T\Delta S$ contribution (Table 1, Fig. 1C).

To understand the structural basis of the Scribble: Tax1 interaction, we determined the crystal structures of PDZ1, PDZ2, and PDZ3 bound to the Tax1 PBM (K^{-7}-H^{-6}-F^{-5}-R^{-4}-E^{-3}-T^{-2}-E^{-1}-V^{0}; Fig. 2, Table 2). As previously shown the Scribble PDZ domains adopt a compact globular fold comprising five to six β-strands and two α-helices that form a β-sandwich structure when engaging with the C-terminal PBM [37]. Examination of the SCRIB PDZ1:Tax1 and PDZ3:Tax1 complex showed that the Tax1 peptide is bound in the canonical ligand-binding groove formed by the β2 strand and helix α2 (Fig. 3). A superimposition with the SCRIB PDZ1: β-PIX (PDB ID: 5VWK) yielded an overall root-mean-square deviation (RMSD) between SCRIB PDZ1:β-PIX and Tax1 complexes of 0.72 Å (Fig. 3). SCRIB PDZ3:Tax1 closely resembles the previously determined structure of

Table 1. Interactions of SCRIB PDZs with Tax1 PBM and superpeptide control. All affinities were measured using isothermal titration calorimetry, with K_D values given in μM and ΔG, ΔH, and $-T\Delta S$ given in kcal·mol^{-1} as a mean of three independent experiments with SD. (A) consists of wild-type SCRIB PDZ domains and SCRIB PDZ mutants against the Tax1 PBM. (B) shows wild-type SCRIB PDZ domains against the superpeptide. N, stoichiometry; NB, no binding.

(A)

	PBM peptide				
	Tax1 (KHFRETEV)				
SCRIB PDZ constructs	*N*	K_D (μM)	ΔG (kcal·mol^{-1})	ΔH (kcal·mol^{-1})	$-T\Delta S$ (kcal·mol^{-1})
PDZ1	1.1 ± 0.02	7.8 ± 0.8	−6.95 ± 0.06	−4.21 ± 0.61	2.75 ± 0.67
PDZ2	1.1 ± 0.01	15.4 ± 1.2	−6.59 ± 0.03	−4.08 ± 0.06	2.51 ± 0.09
PDZ3	0.9 ± 0.07	9.1 ± 0.7	−6.87 ± 0.04	−13.3 ± 0.08	−6.41 ± 0.13
PDZ4	1.0 ± 0.13	40.2 ± 3.1	−6.82 ± 0.46	−2.17 ± 0.90	4.13 ± 0.44
PDZ1 H793A	NB	NB	NB	NB	NB
PDZ2 H928A	NB	NB	NB	NB	NB
PDZ3 H1071A	NB	NB	NB	NB	NB
PDZ4 R1110D	NB	NB	NB	NB	NB
PDZ4 R1116D	NB	NB	NB	NB	NB
PDZ4 H1170A	NB	NB	NB	NB	NB

(B)

	PBM Peptide				
	Super-peptide (RSWFETWV)				
SCRIB PDZ constructs	*N*	K_D (μM)	ΔG (kcal·mol^{-1})	ΔH (kcal·mol^{-1})	$-T\Delta S$ (kcal·mol^{-1})
PDZ1	0.9 ± 0.01	0.6 ± 0.04	−8.46 ± 0.02	−3.72 ± 0.07	−4.74 ± 0.08
PDZ2	1.0 ± 0.03	2.2 ± 0.7	−7.74 ± 0.19	−7.04 ± 0.60	−0.005 ± 0.80
PDZ3	0.9 ± 0.02	1.6 ± 0.2	−7.90 ± 0.05	−11.31 ± 0.10	3.41 ± 0.15
PDZ4	1.1 ± 0.07	12.6 ± 4.3	−6.70 ± 0.21	−2.90 ± 0.86	−3.69 ± 0.65

SCRIB PDZ3:β-PIX complex (PDB ID 5VW1), with the overall RMSD of 0.28 Å when superimposed (Fig. 3).

Unexpectedly, the SCRIB PDZ2:Tax1 complex revealed an unusual binding mode where the β-stranded shaped Tax1 peptide is located antiparallel between the β2 strand of one PDZ2 molecule (Chain A) and the β3 of another PDZ2 molecule (Chain B) in the same asymmetric unit, foring a beta-sheet between Chain A β2-Tax1-Chain B β3. In this complex, Chain A formed hydrogen bonds between Val353 (carboxyl terminus)^{Tax1}-Leu872 (backbone)^{PDZ2},Val353 (carboxyl-terminus)^{Tax1}-Gly873^{PDZ2}, Val353 (carboxyl-terminus)^{Tax1}-Phe874 (backbone)^{PDZ2}, Thr351 (backbone)^{Tax1}-Ile876 (backbone)^{PDZ2}, Glu350 (carboxyl side chain)^{Tax1}-Gly878^{PDZ2}, and His347 (backbone)^{Tax1}-Thr883^{PDZ2} (Fig. 3). Chain B only contributed 2 residues that bound to the peptide: backbone-mediated contacts involving Glu352^{Tax1}-Ile897^{PDZ2} and Thr351^{Tax1}-Glu899^{PDZ2} (Fig. 3). Interestingly, there is a hydrogen bond between Chain B Arg867 and Chain A Tyr885 side chains (Fig. 3) located in loop regions that contributes to the PDZ2 dimer. Despite this unusual 2 : 1 stoichiometry, no significant differences are observed in the overall PDZ domain fold when each of the two PDZ2 molecules are superimposed against the previously determined SCRIB PDZ2:VANGL2 complex (Fig. 3). Chain A showed an overall RMSD of 0.920 and 0.847 Å, while Chain B showed an overall RMSD of 0.955 and 0.823 Å (Fig. 3).

Since we observed this dimerization of PDZ2, we subjected PDZ2 on its own as well as in complex with the Tax1 PBM peptide to analytical ultracentrifugation (AUC) (Fig. 4). For PDZ2 alone, the presence of a single, broad peak spanning molecular weights corresponding to both monomeric and dimeric forms of PDZ2 suggests that PDZ2 exists in a rapid monomer-dimer equilibrium. Moreover, the shifting of this peak towards lower molecular weights upon the addition of Tax1 suggests that the dimeric form is less favoured when PDZ2 is in the ligand bound form.

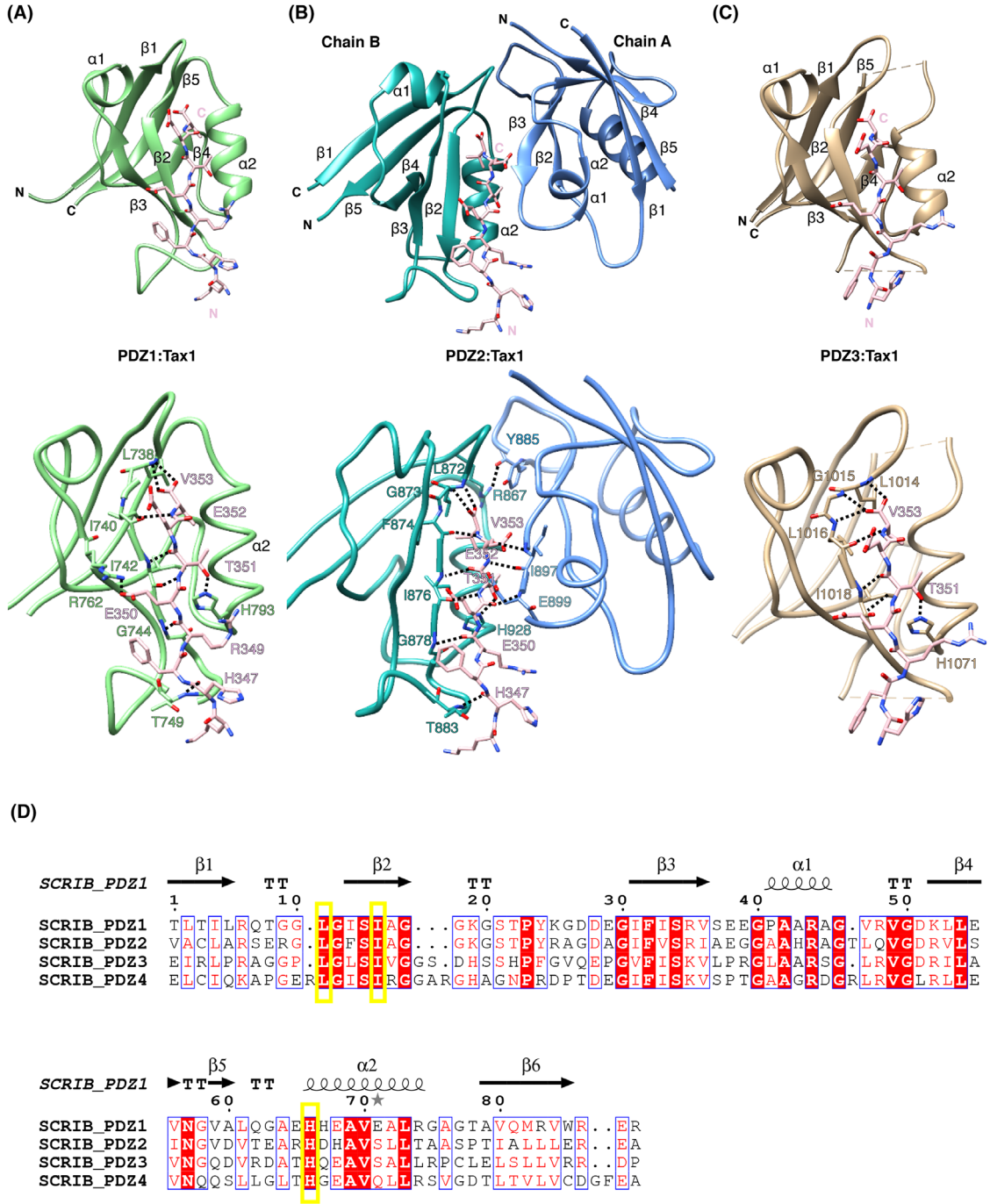

Fig. 2. The crystal structures and detailed interactions of PDZ1, PDZ2, and PDZ3 bound to Tax1 peptide (purple). (A) SCRIB PDZ1 (green) is shown as a cartoon with Tax1 PBM peptide (magenta) shown as sticks. Hydrogen bonds are shown as black dotted lines. (B) PDZ2 Chain A (light sea green) and Chain B (cornflower blue) shown as a cartoon with Tax1 peptide (magenta) as sticks. Front view of PDZ2 interactions via with Chain A (light sea green) and Chain B (cornflower blue) with the Tax1 peptide shown as trace and sticks. Hydrogen bonds are shown as black dotted lines. (C) PDZ3 (gold) shown as a cartoon with Tax1 peptide (magenta) as sticks. Hydrogen bonds are shown as black dotted lines. (D) Sequence alignment of human Scribble PDZ domains (Uniprot Q14160). Conserved residues are shaded in lilac, key residues that are involved in Tax1 PBM interaction are boxed in yellow. Alignment generated using ESPript (http://espript.ibcp.fr/ESPript/cgi-bin/ESPript.cgi) using the sequences of individual Scribble PDZ domains (Uniprot Q14160). Residues coloured in red are conserved and non-coloured have different residues. Secondary structures are shown above the alignment based on PDZ1 (PDB ID: 5VWC); β stands for beta strands, α are the alpha helix, and TT represents turns within the structure. All images of structures were generated using Chimera [70].

Table 2. X-ray data collection and refinement statistics.

	PDZ1:Tax1	PDZ2:Tax1	PDZ3:Tax1
Data collection			
Space group	P 6_1	P 6_1 2 2	P 2_1
No. of molecules in AU	2	2 + 1	2
Cell dimensions			
a, b, c (Å)	50.26, 50.26, 184.40	100.77, 100.77, 68.53	37.74, 44.22, 60.64
α, β, γ (°)	90.00, 90.00, 120.00	90.00, 90.00, 120.00	90.00, 93.44, 90.00
Wavelength (Å)	0.95	0.95	0.95
Resolution (Å)[a]	46.10–1.77 (1.80–1.77)	53.89–1.9 (1.94–1.90)	44.22–1.87 (1.91–1.87)
Rsym or Rmerge[a]	0.056 (0.76)	0.086 (1.89)	0.064 (1.32)
I/σI[a]	16.48 (1.59)	8.50 (0.80)	11.3 (0.8)
CC(1/2)	0.99 (0.43)	0.99 (0.44)	0.99 (0.58)
Completeness (%)[a]	99.3 (97.9)	98.9 (97.8)	99.2 (88.6)
Redundancy[a]	2.7 (2.7)	5.4 (5.7)	6.8 (6.6)
Wilson B-factor	31.33	38.14	33.29
Refinement			
Resolution (Å)	28.14–1.77 (1.83–1.77)	53.89–1.9 (1.97–1.90)	31.14–1.85 (1.91–1.85)
No. of reflections	25 395 (2557)	16 417 (1586)	16 498 (1313)
R_{work}/R_{free}	0.22/0.26	0.21/0.25	0.22/0.28
No. of non-hydrogen atoms			
Protein	1636	1395	1339
Ligand/ion	42	26	53
Water	156	121	178
B-Factors			
Protein	45.59	44.56	37.49
Ligand/ion	68.62	102.22	0
Water	49.42	52.41	38.11
R.m.s. deviations			
Bond lengths (Å)	0.011	0.008	0.014
Bond angle (°)	0.95	1.16	1.41
Ramachandran plot (%)			
Favoured	99.52	98.92	98.12
Allowed	0.48	1.08	1.88
Disallowed	0	0	0

[a]Values in parentheses are for the highest resolution shell.

In the PDZ1:Tax1 complex, Val353^{Tax1} is docked in the conserved hydrophobic pocket formed by PDZ1 Leu738, Ile740 and Ile742. In addition, four hydrogen bonds are formed by Glu352 (backbone)^{Tax1}–Ile740 (backbone)^{PDZ1}, Thr351^{Tax1}–His793^{PDZ1}, His347(backbone)^{Tax1}–Thr749(backbone)^{PDZ1}, and Arg349 (backbone)^{Tax1}-Gly744(backbone) ^{PDZ1} (Fig. 3). A salt bridge is also formed between Glu350^{Tax1}-Arg762 ^{PDZ1}, in which the Arg762 ^{PDZ1} side chain extends from the 3rd beta sheet of PDZ1 to make contact with the Glu350^{Tax1} side chain (Fig. 3). The structure of PDZ3:Tax1 revealed Tax1 Val353 forming several hydrogen bonds via its C-terminal carboxyl group with PDZ3 at the carboxyl loop-binding region including Leu1014, Gly1015, and Leu1016, which all contribute via the peptide backbone. Furthermore, Thr351^{Tax1} formed a backbone-mediated hydrogen bond with Ile1018^{PDZ3} of the β2 as well as Thr351^{Tax1} side chain-mediated hydrogen bond with 1071His^{PDZ3} located on the α2 helix (Fig. 3).

To validate our crystal structures, we performed mutagenesis to probe Scribble PDZ domain interactions with Tax1 PBM in ITC (Table 1, Figs 5 and 6). The equivalent structure guided mutants PDZ1 H793A, PDZ2 H928A, and PDZ3 H1071A, all showed no binding, suggesting that the common His within the active-binding site of the PDZ:Tax1 complexes may play a pivotal role in complex formation (Table 1, Figs 4–6).

In the absence of a crystal structure of SCRIB PDZ4 bound to Tax1 PBM, we modelled a putative PDZ4:Tax1 PBM complex by superimposing the SCRIB PDZ1:Tax1 complex on SCRIB PDZ4. This suggested PDZ4 R1110, R1111, and H1170 as potential interactors with Tax1 PBM. SCRIB PDZ4 mutants bearing one of each mutation (PDZ4

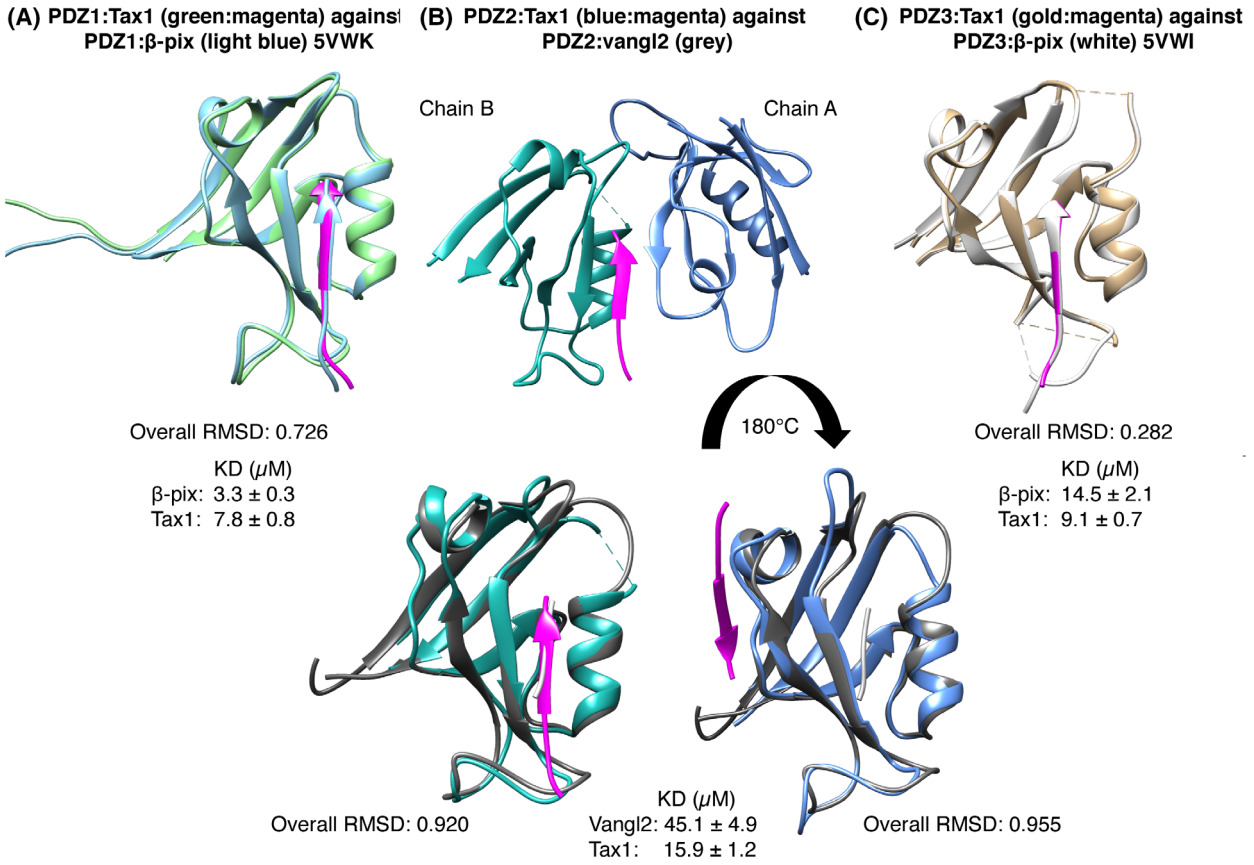

Fig. 3. Superimposition of SCRIB PDZ:Tax1 complexes with SCRIB PDZ complex structures bound to host PBM peptides. (A) PDZ1:Tax1 (green:magenta) with PDZ1:β-PIX (light blue, PDB ID 5VWK). (B) PDZ2:Tax1 Chain A (light sea green:magenta) and Chain B against PDZ2:VANGL2 (sandy brown). (C) PDZ3:Tax1 (gold:magenta) against PDZ3:β-PIX (yellow, PDB ID 5VWK). All protein chains are shown as cartoon. All images of structures were generated using the Chimera [70].

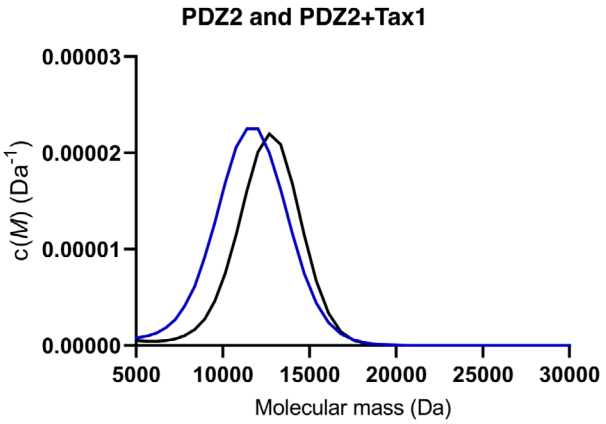

Fig. 4. Sedimentation velocity analyses by analytical ultracentrifugation of apo SCRIB PDZ2 (black line) and SCRIB PDZ2 + Tax1 (blue line).

R1110D, PDZ4 R1116D, and PDZ4 H1170A) were folded (Fig. 6) but did not show detectable binding to Tax1 (Table 1; Fig. 4).

Discussion

Scribble is a crucial cell polarity regulator that mediates signalling pathways via its PDZ domains [2,11]. As a result, Scribble and other PDZ domain-containing proteins play a pivotal role in disease and consequently are targeted by viruses to allow them to establish a cellular environment that supports viral replication [15,38–40]. HTLV-1 encodes for the oncogenic protein Tax1, which features a PBM at its C-terminus that substantially impacts the oncogenic activity of Tax1 [41].

Human Scribble has previously been shown to directly interact with the Tax1 C-terminal PBM via PDZ2 and PDZ4 using a β-galactosidase assay, however another study using synthetic fluorescein-labelled peptide assays demonstrated interactions with PDZ2 and PDZ3 [41,42]. In our hands, the Tax1 PBM binds to all four Scribble PDZ domains when examined using isothermal titration calorimetry. The affinities of Tax1 to Scribble PDZ domains display a distinct

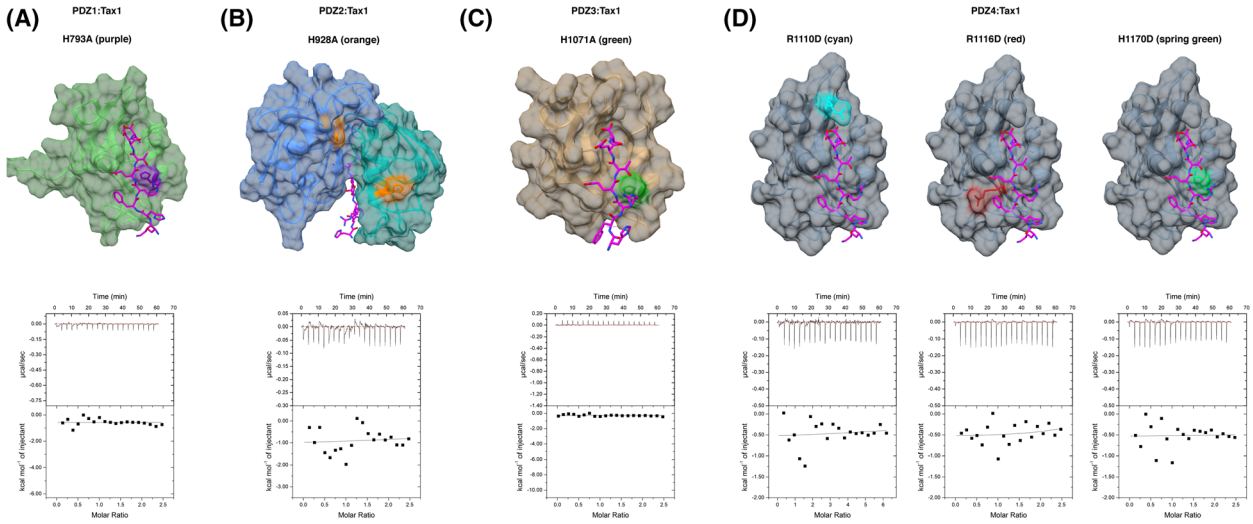

Fig. 5. Location of Scribble PDZ domain mutations. Mutated residues are coloured on a surface representation of the relevant Scribble PDZ domain constructs. Binding profiles of isolated mutant Scribble PDZ domain interactions with Tax1 peptide. Each profile is represented by a raw thermogram and a binding isotherm fitted with a one-site binding model (bottom panels). Each of the values was calculated from at least three independent experiments. (A) PDZ1 H793A (purple) (B) PDZ2 H928A (orange). (C) PDZ3 H1071A (green). (D) PDZ4 R1110D (cyan), PDZ4 R1116D (red), and PDZ4 H1170D (spring green). SCRIB PDZ4:Tax1 homology model complex was generated with Chimera 1.14.

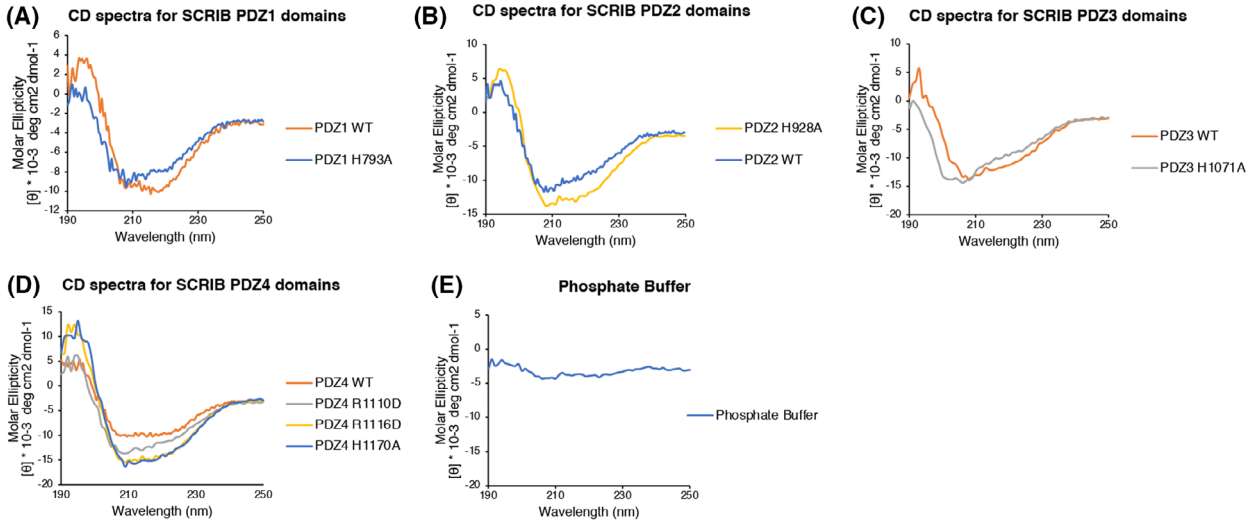

Fig. 6. Circular dichroism spectroscopy of wild type and mutant SCRIB PDZ1, 2, 3, and 4 mutants. (A–E) Circular dichroism spectra recorded for wild type and mutant SCRIB PDZ1, 2, 3, and 4 domains indicated that there were no major spectral differences between the proteins, suggesting that they were similarly folded, with mutations not leading to unfolding of the PDZ domains.

hierarchy, with PDZ3 being the tightest binder (K_D = 9.1 μM), whereas Tax1 binding to PDZ1 (K_D = 7.8 μM), PDZ2 (K_D = 15.4 μM), and PDZ4 (K_D = 40.2 μM) is weaker. Mutagenesis of key interacting residues of Scrib PDZ domains with Tax1 revealed that a conserved His found in PDZ1 H793, PDZ2 H928, and PDZ3 H1071 on the α2 of each domain is a major determinant of the interaction, since mutation to an Ala abolished binding as measured by ITC. Interestingly, we also observed loss of binding with a PDZ4 H1170A mutant. However, mutation of all residues identified as putative interactors in the PDZ4-binding groove resulted in loss of binding, suggesting that PDZ4 may inherently be more susceptible to disruption.

A comparison of the crystal structures of PDZ1, PDZ2, and PDZ3 bound to Tax1 revealed multiple conserved interactions consistent with previous

observations for canonical class I PBM interactions with PDZ domains. All the complexes featured an Ile^{PDZ}-$Thr351^{Tax1}$ and Leu^{PDZ}-$Val353^{Tax1}$ hydrogen bond located on the second beta-strand of the PDZ domain (Figs 1 and 3). Furthermore, a conserved Thr at the C-terminal end of β2 of PDZ1 (Thr749) and PDZ2 (Thre883) forms a hydrogen bond with $His347^{Tax1}$ (Fig. 3). Lastly, the conserved His in each domain found on α2, PDZ1 H793, PDZ2 H928, and PDZ3 H1071, shared a hydrogen bond with $Thr351^{Tax1}$, and mutation to Ala ablates Tax1 binding to SCRIB PDZ domains as seen in our ITC analysis (Table 1, Figs 1B and 3). This particular conserved His residue is also involved in interactions with other cellular and viral interactors of Scribble as observed in crystal structures of SCRIB PDZ1:β-PIX, PDZ3:β-PIX, PDZ1:MCC, PDZ1:APC, PDZ1:Vangl2, PDZ2:Vangl2, PDZ3:Vangl2, PDZ1: NS1, and PDZ3:NS1 [20,37,43–45], thus making this residue vital for SCRIB:ligand interactions.

We previously observed SCRIB binding to interactors such as β-PIX only with a distinct pattern, where tight binding was observed for PDZ1 and PDZ3 domains, and only weaker binding to PDZ2 and no binding to PDZ4 [37], whereas Tax1 is able to bind to all SCRIB PDZ domains. Superimposition of PDZ3:Tax1 and PDZ3:β-PIX yielded an RMSD of 0.282 Å, suggesting that binding to these interactors does not require changes in secondary structure elements, and that the differences in affinities and interaction pattern between β-PIX and Tax1 are due to differential contact formation with each PBM. β-PIX and Tax1 form different hydrogen bond networks with PDZ3. In PDZ3:β-PIX, $Asn645^{β\text{-}PIX}$ interacts with $Ser1017^{PDZ3}$, whereas in PDZ3:Tax1, $Val353^{Tax1}$ interacts with $Leu1014^{PDZ3}$, $Gly1015^{PDZ3}$, and $Leu1016^{PDZ3}$ [37], and these differential interactions ultimately provide a basis for ligand discrimination.

Since we were unable to determine a crystal structure of a PDZ4:Tax1 complex, we predicted based on the structures we obtained several putative interacting residues in PDZ4 that were targeted for mutagenesis. Interestingly, PDZ4 R1110D, PDZ4 R1116D, and PDZ4 H1170A mutants did not bind to Tax1, suggesting that all may play a significant role in PDZ4:Tax1 binding. PDZ4 displayed the weakest affinity (40.2 ± 3.1 μM) compared with all other Scrib PDZ domains; however, Tax1 is one of the the first biological interactors (i.e. not synthetic) we have been able to verify using purified protein and peptides. Although others have reported SCRIB PDZ4 binding to multiple interactors, we have not been able to confirm these interactions with the TBEV NS5, HPV-16 E6, and β-PIX [37] (our unpublished data). None of the reported interactions are solely PDZ4 specific, with ZO-2, DLC3, GluN2A, GluN2B, and NOS1AP binding to other SCRIB PDZ domains as well as PDZ4 [46–49].

Strikingly, we observed that two PDZ2 molecules bound to one Tax1 peptide at the interface between the two PDZ2 chains, revealing a potential novel site for SCRIB PDZ domain engagement. Canonical binding of a C-terminal PBM to a PDZ domain utilizes the carboxyl loop sandwiched between the β2 and α2 that forms a hydrophobic pocket for the C-terminal residue in the PBM peptide to bind into [37,43,44]. Unexpectedly, a neighbouring PDZ2 molecule also engaged Tax1 PBM via the β3-strand, leading to the formation of a contiguous β-sheet between Chain A β2-Tax1-Chain B β3. However, ITC analysis revealed that SCRIB PDZ2 binds the Tax1 PBM with a stoichiometry of 1 : 1, suggesting that in the presence of Tax1 PBM PDZ2 is monomeric in solution and only forms a heterodimer and not a heterotrimer. This was further supported with our AUC data (Fig. 4) showing that PDZ2 exists in a rapid monomer–dimer equilibrium, with Tax1-bound protein favouring the monomeric form. Although the crystal structure shows a dimer with the Tax1 peptide, this alternative binding site is unlikely to be used in solution and likely a crystallization artefact.

Our data focuses on the interactions of Tax1 PBM with individual Scribble PDZ domains. Although providing mechanistic insight into these interactions, our findings do not shed light onto the architecture of a Scribble:Tax1 complex featuring longer fragments or indeed full-length proteins. No full-length structures of Tax1 or Scribble are currently available. However, with Scribble features four PDZ domains with the capacity to interact with partners, differential regulation of interactions may occur via ligand competition and/or PDZ-binding groove accessibility. Furthermore, there is evidence that Scribble PDZ3 and PDZ4 domains work together as a unit featuring a single binding site, with interacting peptides primarily binding to the αB/βB pocket of PDZ3, whereas PDZ4 was effectively used to expand the PDZ3-binding grove to create an elongated site within the supramodule, thus providing another level of structural regulation within the PDZ domains [50].

An additional level of complexity to cell polarity regulation is provided by posttranslational modifications such as via phosphorylation of PBMs [39,51–53]. In particular, Scribble has been shown to be subject to modulation of interactions by phosphorylation, including virus encoded interactors such as HPV-16 E6 and HTLV-1 Tax1 which were shown to be

phosphorylated at the −2 position of their PBM with phosphorylation inhibiting PDZ recognition [51,52]. In our structures, Tax Thr351 which occupies the −2 position in the PBM forms a side chain-mediated hydrogen bond with a His from interacting SCRIB PDZ domains, thus providing a structural rationale for this observation. We note that phosphorylation does not always affect the affinity of an interaction, with the SCRIB:MCC (Mutated in Colorectal Cancer) interaction largely unaffected, without a significant difference in SCRIB PDZ1 and PDZ3 affinities for phosphorylated vs native MCC PBM [43]. Consequently the detailed role of phosphorylation on the Scribble: Tax1 interaction requires further investigation.

In summary, we show that Scribble PDZ domains display differential binding affinities for HTLV-1 Tax1 and that subtle differences in the detailed interactions drive the differences in affinity observed for PDZ1, PDZ2, and PDZ3. Our findings provide a structural basis for HTVL-1 Tax1 subversion of Scribble-mediated polarity signalling and will form the platform for future structure-guided investigations to understand how the differential ability of individual Scribble PDZ domains to engage Tax1 impacts the control of cell polarity during viral replication.

Materials and methods

Protein expression and purification

Human Scribble (SCRIB) PDZ1 (728–815), PDZ2 (860–950), PDZ3 (1002–1094), and PDZ4 (1099–1203) domain proteins (Uniprot accession number: Q14160) as well as mutant SCRIB PDZ domain proteins were purified as previously described [37,45]. SCRIB PDZ mutants cDNA PDZ3 H1071A (residues 1002–1094), PDZ4 R1110D (residues 1099–1203), PDZ4 R1116D (residues 1099–1203), and PDZ4 H1170A (residues 1099–1203) was cloned into the pGex-6P3 vector (Bioneer). All other SCRIB PDZ mutant constructs were described previously [37]. All other SCRIB PDZ WT constructs were also described previously [37].

Target proteins were expressed using *E. coli* BL21 (DE3) pLysS cells (BIOLINE) 2YT media (1.6% w/v Tryptone, 1.0% w/v Yeast Extract and 0.5% w/v sodium chloride [NaCl]) supplemented with 100 $\mu g \cdot mL^{-1}$ ampicillin at 37 °C and shaken at 160 rpm for approximately 20 h. Protein expression was induced using the auto-induction protocol [54]. His-MBP-tagged proteins were purified via immobilized metal affinity chromatography, using HisTrap HP columns (GE Healthcare, Chicago, IL, USA). GST-tagged proteins were purified using glutathione Sepharose 4B resins (GE Healthcare). His-MBP constructs were cleaved with His-MBP TEV protease and GST constructs were cleaved with GST-3C protease overnight at 4 °C. All constructs were subjected to size exclusion chromatography using a Superdex 75 10/300 column (GE Healthcare) equilibrated within 20 mM HEPES, 150 NaCl, pH7.2 using the AKTA Pure. All proteins were purified as previously described [37]. The concentration of SCRIB PDZ1 was determined at Abs280 nm using a NanoDrop 2000/2000c Spectrophotometer (Thermo Fisher Scientific, Scoresby, Victoria, Australia). All other proteins lacked a Tryptophan residue, and concentrations were quantified using Abs205 nm via the Scopes method [55].

Peptides

Peptides used for ITC and crystallization were Tax1: KHFRETEV (UniProt accession code P14079, residues 346–353) (Genscript) and superpeptide: RSWFETWV [46] (Mimotopes).

Analytical ultracentrifugation

Sedimentation velocity experiments were performed at 25 °C in a Beckman Coulter XL-A analytical ultracentrifuge as described previously [56–59]. Briefly, double sector cells containing synthetic quartz windows were loaded with 400 μL of reference buffer (25 mM HEPES pH 7.5, 150 mM NaCl) and 380 μL of apo protein at 92 μM or 380 μL of protein:ligand in a 1 : 4 ratio at 92 μM : 367 μM (solubilized in buffer). The cells were loaded into an 8-hole An50-Ti rotor before centrifugation at 145 000 ***g***. Data were collected continuously at 230 nm using a radial step size of 0.003 cm without averaging. Solvent density (1.006 $g \cdot mL^{-1}$), solvent viscosity (0.0103091 cp) and estimated protein partial specific volume (0.736344 $mL \cdot g^{-1}$) were calculated using SEDNTERP [60]. Absorbance was fitted as a function of radial position to the Lamm equation using SEDFIT to determine the continuous mass (c (M)) distributions [61–63].

Measurement of dissociation constants

Binding affinities were measures using PDZ domain constructs in 20 mM HEPES, 150 NaCl, pH7.2 at a final concentration of 75 μM. Peptide ligands were used at a concentration of 900 μM, and all affinity measurements were performed in triplicate. Peptide concentrations were calculated based on the dry peptide weight after synthesis. ITC experiments were conducted using a MicroCal iTC200 System (GE Healthcare) at 25 °C with a stirring speed of 750 rpm using 20 injections. Data were analysed using the Origin 7.0 software (OriginLab Corporation, Northampton, MA, USA) using "one-site binding. model". Superpeptide was used as a positive control and titrations of peptide against buffer (20 mM HEPES, 150 NaCl, pH7.2) were performed as a negative control.

Crystallization and structure determination

Complexes of SCRIB PDZ domains with Tax1 peptide were reconstituted as described previously [64]. Briefly, protein and peptide were mixed at a molar ratio of 1 : 4 and then concentrated to 10 mg·mL^{-1} using 3 kDa cut-off Ultra-0.5 centrifugal filter units (Millipore, Burlington, MA, USA) at 4 °C. Concentrated protein complex samples were subjected to high-throughput crystallization screening using a Gryphon LCP (Art Robbins Instruments) with 0.2 μL of protein sample and 0.2 μL reservoir solution per drop and the following sparse matrix screens; JCSG-plus: HT-96 sparse matrix screen (Molecular Dimensions, Rotherham, UK), PACT Premier HT-96 sparse matrix screen (Molecular Dimensions), Structure Screen 1 + 2 sparse matrix screen (Molecular Dimensions) and Salt Rx sparse matrix screen (Hampton Research, Aliso Viejo, CA, USA). Identified crystallization conditions were optimized using a grid screen approach in 24-well sitting drop plates (Hampton Research) at 20 °C with a drop size of 2 μL comprising 1 μL of protein sample and 1 μL of reservoir solution.

Crystals were mounted on nylon and copper loops (MiTGen, Ithaca, NY, USA). All data were collected at the Australian Synchrotron using the MX2 beamline equipped with the Eiger 16M detector (Dectris) with an oscillation range 0.1° per frame with a wavelength of 0.9537, integrated using XDS [65] and scaled using AIMLESS [66].

SCRIB PDZ1:Tax1 crystals were grown in 0.1 M zinc chloride, 0.1 M sodium acetate pH 5.0, 20% w/v PEG 1500, and flash cooled at −173 °C in mother liquor supplemented with 30% glucose. The SCRIB PDZ1:Tax1 complex formed single hexagonal rod-shaped crystal belonging to space group $P6_5$ with a = 50.26 Å, b = 50.26 Å, c = 184.40 Å, α = 90.00°, β = 90.00°, and γ = 120° in the hexagonal crystal system. Molecular replacement was carried out using PHASER [67] with the previously solved structure of SCRIB PDZ1: β-PIX (PDB ID: 5VWK) [37] as a search model. SCRIB PDZ1:Tax1 crystals contained 2 molecules each of PDZ1 and Tax1 peptide in the asymmetric unit, with 40.66% solvent content. The final TFZ and LLG values after molecular replacement were 27.3 and 714, respectively. The final model was built manually over several cycles using Coot [68] and refined using PHENIX with a final R_{work}/R_{free} of 0.22/0.26, with 99.52% of residues in the favoured region of the Ramachandran plot and 0% of rotamer outliers.

SCRIB PDZ2:Tax1 crystals were grown in 2.0 M Ammonium sulfate, 20% w/v PEG 3350 and were flash cooled at −173 °C in mother liquor supplemented with 30% glucose. The SCRIB PDZ2:Tax1 complex formed single ovoid disc shaped crystals belong to space group $P6_122$ with a = 100.77 Å, b = 100.77 Å, c = 68.53 Å, α = 90.00°, β = 90.00°, and γ = 120.00° in the hexagonal crystal system. Molecular replacement was carried out using PHASER [67] with the previously solved structure of SCRIB PDZ2 [45] as a search model. SCRIB PDZ2:Tax1 crystals contained 2 molecules of PDZ2 and 1 molecule of Tax1 peptide in the asymmetric unit, with 42.82% solvent content and final TFZ and LLG values of 23.1 and 507.5, respectively. Model building and refinement were performed as above with final R_{work}/R_{free} of 0.22/0.26, with 99.44% of residues in the favoured region of the Ramachandran plot and no rotamer outliers.

SCRIB PDZ3:Tax1 crystals were grown in 0.1 M HEPES pH 7, 30% v/v Jeffamine and were flash cooled at −173 °C in mother liquor supplemented with 30% glycerol. The SCRIB PDZ3:Tax1 complex formed single trigonal prism-shaped crystals belong to space group $P2_1$ with a = 37.74 Å, b = 43.22 Å, c = 60.64 Å, α = 90.00°, β = 93.44°, and γ = 90.00° in the monoclinic crystal system. Molecular replacement was carried out using PHASER [67] with the previously solved structure of SCRIB PDZ3: β-PIX (PDB ID: 5VWI) [37] as a search model. SCRIB PDZ3:Tax1 crystals contained 2 molecules each of PDZ3 and Tax1 peptide in the asymmetric unit, with 51.88% solvent content and final TFZ and LLG values of 21.7 and 569.38, respectively. Model building and refinement were performed as above with final R_{work}/R_{free} of 0.22/0.28, with 98.12% of residues in the favoured region of the Ramachandran plot and no outliers.

SCRIB PDZ4 modelling

SCRIB PDZ4:Tax1 model complex was generated with Chimera 1.14 by superimposing the tax peptide from the SCRIB PDZ1:Tax1 complex on a previously solved structure of SCRIB PDZ4 (PDB:4WYT) [50] (Fig. 5). SCRIB PDZ1 (48.86%) has the highest sequence similarity to SCRIB PDZ4 compare to SCRIB PDZ2 (37.08%) and PDZ3 (44.44%) (CLUSTAL2.1, https://www.ebi.ac.uk/Tools/msa/clustalo/).

Acknowledgements

We thank the staff at the MX beamlines at the Australian Synchrotron for help with X-ray data collection. We thank the ACRF for their support of the Eiger MX detector at the Australian Synchrotron MX2 beamline and the Comprehensive Proteomics Platform at La Trobe University for core instrument support. This research was funded by the Australian Research Council (Fellowship FT130101349 to MK), National Health and Medical Research Council of Australia (Project Grant APP1007918 to MK and POH), La Trobe University (Scholarships to AJJ, JCM and ERRM). ERRM is the recipient of a Grains Research and Development Corporation scholarship (grant no. 9176977). Open access publishing facilitated by La Trobe University, as part of the Wiley - La

Trobe University agreement via the Council of Australian University Librarians.

Conflict of interest

The authors declare no conflict of interest.

Author contributions

AJ: Acquisition of data; Analysis and interpretation of data; Drafting and revising the article. JCM: Acquisition, analysis and interpretation of data, Drafting and revising the article. ERRM: Acquisition, analysis and interpretation of data, Drafting and revising the article. TPSC: Acquisition, analysis and interpretation of data, Drafting and revising the article. POH: Conception and design; Analysis and interpretation of data; Drafting and revising the article. MK: Conception and design; Acquisition of data; Analysis and interpretation of data; Drafting and revising the article.

Data availability statement

Coordinate files have been deposited in the Protein Data Bank under the accession codes 7QS8, 7QRT, and 7QRS. All raw diffraction images were deposited on the SBGrid Data Bank [69] using their PDB accession codes.

References

1 Nelson WJ. Adaptation of core mechanisms to generate cell polarity. *Nature*. 2003;**422**(6933):766–74.
2 Stephens R, Lim K, Portela M, Kvansakul M, Humbert PO, Richardson HE. The scribble cell polarity module in the regulation of cell signaling in tissue development and tumorigenesis. *J Mol Biol*. 2018;**430**:3585–612.
3 Krummel MF, Macara I. Maintenance and modulation of T cell polarity. *Nat Immunol*. 2006;**7**(11):1143–9.
4 Royer C, Lu X. Epithelial cell polarity: a major gatekeeper against cancer? *Cell Death Differ*. 2011;**18**(9):1470–7.
5 Allam AH, Charnley M, Russell SM. Context-specific mechanisms of cell polarity regulation. *J Mol Biol*. 2018;**430**(19):3457–71.
6 Tahirovic S, Bradke F. Neuronal polarity. *Cold Spring Harb Perspect Biol*. 2009;**1**(3):a001644.
7 Jarjour AA, Boyd A, Dow LE, Holloway RK, Goebbels S, Humbert PO, et al. The polarity protein scribble regulates myelination and remyelination in the central nervous system. *PLoS Biol*. 2015;**13**(3):e1002107.
8 Ludford-Menting MJ, Oliaro J, Sacirbegovic F, Cheah ETY, Pedersen N, Thomas SJ, et al. A network of PDZ-containing proteins regulates T cell polarity and morphology during migration and immunological synapse formation. *Immunity*. 2005;**22**(6):737–48.
9 Bryant PJ, Huwe A. LAP proteins: what's up with epithelia? *Nat Cell Biol*. 2000;**2**(8):E141–3.
10 Albertson R, Chabu C, Sheehan A, Doe CQ. Scribble protein domain mapping reveals a multistep localization mechanism and domains necessary for establishing cortical polarity. *J Cell Sci*. 2004;**117**(25):6061–70.
11 Lee HJ, Zheng JJ. PDZ domains and their binding partners: structure, specificity, and modification. *Cell Commun Signal*. 2010;**8**:8.
12 Giallourakis C, Cao Z, Green T, Wachtel H, Xie X, Lopez-Illasaca M, et al. A molecular-properties-based approach to understanding PDZ domain proteins and PDZ ligands. *Genome Res*. 2006;**16**(8):1056–72.
13 Pike KA, Kulkarni S, Pawson T. Immature T-cell clustering and efficient differentiation require the polarity protein Scribble. *Proc Natl Acad Sci USA*. 2011;**108**(3):1116–21.
14 Chang JT, Palanivel VR, Kinjyo I, Schambach F, Intlekofer AM, Banerjee A, et al. Asymmetric T lymphocyte division in the initiation of adaptive immune responses. *Science*. 2007;**315**(5819):1687–91.
15 Javier RT, Rice AP. Emerging theme: cellular PDZ proteins as common targets of pathogenic viruses. *J Virol*. 2011;**85**(22):11544–56.
16 Fan S, Macken CA, Li C, Ozawa M, Goto H, Iswahyudi NFN, et al. Synergistic effect of the PDZ and p85beta-binding domains of the NS1 protein on virulence of an avian H5N1 influenza A virus. *J Virol*. 2013;**87**(9):4861–71.
17 Nakagawa S, Huibregtse JM. Human scribble (vartul) is targeted for ubiquitin-mediated degradation by the high-risk papillomavirus E6 proteins and the E6AP ubiquitin-protein ligase. *Mol Cell Biol*. 2000;**20**:8244–53.
18 Werme K, Wigerius M, Johansson M. Tick-borne encephalitis virus NS5 associates with membrane protein scribble and impairs interferon-stimulated JAK-STAT signalling. *Cell Microbiol*. 2008;**10**(3):696–712.
19 Javorsky A, Humbert PO, Kvansakul M. Molecular basis of Tick Born encephalitis virus NS5 mediated subversion of apico-basal cell polarity signalling. *Biochem J*. 2022;**479**(12):1303–15.
20 Javorsky A, Humbert PO, Kvansakul M. Structural basis of the avian influenza NS1 protein interactions with the cell polarity regulator scribble. *Viruses*. 2022;**14**(3):583.
21 Proietti FA, Carneiro-Proietti ABF, Catalan-Soares BC, Murphy EL. Global epidemiology of HTLV-I infection and associated diseases. *Oncogene*. 2005;**24**(39):6058–68.
22 Yasunaga J, Matsuoka M. Molecular mechanisms of HTLV-1 infection and pathogenesis. *Int J Hematol*. 2011;**94**(5):435–42.

23 Matsuoka M, Jeang K-T. Human T-cell leukaemia virus type 1 (HTLV-1) infectivity and cellular transformation. *Nat Rev Cancer*. 2007;**7**(4):270–80.
24 Ahmadi Ghezeldasht S, Shirdel A, Assarehzadegan MA, Hassannia T, Rahimi H, Miri R, et al. Human T lymphotropic virus type I (HTLV-I) oncogenesis: molecular aspects of virus and host interactions in pathogenesis of adult T cell leukemia/lymphoma (ATL). *Iran J Basic Med Sci*. 2013;**16**(3):179.
25 Shirinian M, Kfoury Y, Dassouki Z, el-Hajj H, Bazarbachi A. Tax-1 and Tax-2 similarities and differences: focus on post-translational modifications and NF-κB activation. *Front Microbiol*. 2013;**4**:231–1.
26 Fujii M, Tsuchiya H, Chuhjo T, Akizawa T, Seiki M. Interaction of HTLV-1 Tax1 with p67SRF causes the aberrant induction of cellular immediate early genes through CArG boxes. *Genes Dev*. 1992;**6**(11):2066–76.
27 Zhao LJ, Giam CZ. Human T-cell lymphotropic virus type I (HTLV-I) transcriptional activator, Tax, enhances CREB binding to HTLV-I 21-base-pair repeats by protein-protein interaction. *Proc Natl Acad Sci USA*. 1992;**89**(15):7070–4.
28 Suzuki T, Narita T, Uchida-Toita M, Yoshida M. Down-regulation of the INK4 family of cyclin-dependent kinase inhibitors by tax protein of HTLV-1 through two distinct mechanisms. *Virology*. 1999;**259**(2):384–91.
29 Iwai K, Mori N, Oie M, Yamamoto N, Fujii M. Human T-cell leukemia virus type 1 tax protein activates transcription through AP-1 site by inducing DNA binding activity in T cells. *Virology*. 2001;**279**(1):38–46.
30 Endo K, Hirata A, Iwai K, Sakurai M, Fukushi M, Oie M, et al. Human T-cell leukemia virus type 2 (HTLV-2) tax protein transforms a rat fibroblast cell line but less efficiently than HTLV-1 tax. *J Virol*. 2002;**76**(6):2648–53.
31 Tsubata C, Higuchi M, Takahashi M, Oie M, Tanaka Y, Gejyo F, et al. PDZ domain-binding motif of human T-cell leukemia virus type 1 Tax oncoprotein is essential for the interleukin 2 independent growth induction of a T-cell line. *Retrovirology*. 2005;**2**(1):46.
32 Higuchi M, Tsubata C, Kondo R, Yoshida S, Takahashi M, Oie M, et al. Cooperation of NF-κB2/p100 activation and the PDZ domain binding motif signal in human T-cell leukemia virus type 1 (HTLV-1) Tax1 but not HTLV-2 Tax2 is crucial for interleukin-2-independent growth transformation of a T-cell line. *J Virol*. 2007;**81**(21):11900–7.
33 Pérès E, Blin J, Ricci EP, Artesi M, Hahaut V, van den Broeke A, et al. PDZ domain-binding motif of Tax sustains T-cell proliferation in HTLV-1-infected humanized mice. *PLoS Pathog*. 2018;**14**(3):e1006933.
34 Ohashi M, Sakurai M, Higuchi M, Mori N, Fukushi M, Oie M, et al. Human T-cell leukemia virus type 1 Tax oncoprotein induces and interacts with a multi-PDZ domain protein, MAGI-3. *Virology*. 2004;**320**(1):52–62.
35 Makokha GN, Takahashi M, Higuchi M, Saito S, Tanaka Y, Fujii M. Human T-cell leukemia virus type 1 Tax protein interacts with and mislocalizes the PDZ domain protein MAGI-1. *Cancer Sci*. 2013;**104**(3):313–20.
36 Marziali F, Marina Bugnon Valdano, Clarisse Brunet Avalos, Moriena L, Cavatorta A, Gardiol D. Interference of HTLV-1 tax protein with cell polarity regulators: defining the subcellular localization of the tax-DLG1 interaction. *Viruses*. 2017;**9**(12):355.
37 Lim KYB, Gödde NJ, Humbert PO, Kvansakul M. Structural basis for the differential interaction of Scribble PDZ domains with the guanine nucleotide exchange factor β-PIX. *J Biol Chem*. 2017;**292**(50):20425–36.
38 Zhan L, Rosenberg A, Bergami KC, Yu M, Xuan Z, Jaffe AB, et al. Deregulation of scribble promotes mammary tumorigenesis and reveals a role for cell polarity in carcinoma. *Cell*. 2008;**135**(5):865–78.
39 Thomas M, Banks L. Upsetting the balance: when viruses manipulate cell polarity control. *J Mol Biol*. 2018;**430**(19):3481–503.
40 Javorsky A, Humbert PO, Kvansakul M. Structural basis of coronavirus E protein interactions with human PALS1 PDZ domain. *Commun Biol*. 2021;**4**(1):724.
41 Arpin-André C, Mesnard J-M. The PDZ domain-binding motif of the human T cell leukemia virus type 1 tax protein induces mislocalization of the tumor suppressor hScrib in T cells. *J Biol Chem*. 2007;**282**(45):33132–41.
42 Ivarsson Y, Arnold R, McLaughlin M, Nim S, Joshi R, Ray D, et al. Large-scale interaction profiling of PDZ domains through proteomic peptide-phage display using human and viral phage peptidomes. *Proc Natl Acad Sci USA*. 2014;**111**(7):2542–7.
43 Caria S, Stewart BZ, Jin R, Smith BJ, Humbert PO, Kvansakul M. Structural analysis of phosphorylation-associated interactions of human MCC with Scribble PDZ domains. *FEBS J*. 2019;**286**(24):4910–25.
44 How JY, Caria S, Humbert PO, Kvansakul M. Crystal structure of the human Scribble PDZ1 domain bound to the PDZ-binding motif of APC. *FEBS Lett*. 2019;**593**(5):533–42.
45 How JY, Stephens RK, Lim KYB, Humbert PO, Kvansakul M. Structural basis of the human Scribble–Vangl2 association in health and disease. *Biochem J*. 2021;**478**(7):1321–32.
46 Zhang Y, Yeh S, Appleton BA, Held HA, Kausalya PJ, Phua DCY, et al. Convergent and divergent ligand specificity among PDZ domains of the LAP and zonula occludens (ZO) families. *J Biol Chem*. 2006;**281**(31):22299–311.

47 Métais J-Y, Navarro C, Santoni MJ, Audebert S, Borg JP. hScrib interacts with ZO-2 at the cell–cell junctions of epithelial cells. *FEBS Lett*. 2005;**579**(17):3725–30.
48 Hendrick J, Franz-Wachtel M, Moeller Y, Schmid S, Macek B, Olayioye MA. The polarity protein Scribble positions DLC3 at adherens junctions to regulate Rho signaling. *J Cell Sci*. 2016;**129**(19):3583–96.
49 Piguel NH, Fievre S, Blanc JM, Carta M, Moreau MM, Moutin E, et al. Scribble1/AP2 complex coordinates NMDA receptor endocytic recycling. *Cell Rep*. 2014;**9**(2):712–27.
50 Ren J, Feng L, Bai Y, Pei H, Yuan Z, Feng W. Interdomain interface-mediated target recognition by the Scribble PDZ34 supramodule. *Biochem J*. 2015;**468**(1):133–44.
51 Bidoia C, Mazzorana M, Pagano MA, Arrigoni G, Meggio F, Pinna LA, et al. The pleiotropic protein kinase CK2 phosphorylates HTLV-1 Tax protein in vitro, targeting its PDZ-binding motif. *Virus Genes*. 2010;**41**(2):149–57.
52 Boon SS, Tomaić V, Thomas M, Roberts S, Banks L. Cancer-causing human papillomavirus E6 proteins display major differences in the phospho-regulation of their PDZ interactions. *J Virol*. 2015;**89**(3):1579–86.
53 Seo W, Prehaud C, Khan Z, Sabeta C, Lafon M. Investigation of rabies virus glycoprotein carboxyl terminus as an in vitro predictive tool of neurovirulence. A 3R approach. *Microbes Infect*. 2017;**19**(9–10):476–84.
54 Studier FW. Protein production by auto-induction in high density shaking cultures. *Protein Expr Purif*. 2005;**41**(1):207–34.
55 Scopes RK. Measurement of protein by spectrophotometry at 205 nm. *Anal Biochem*. 1974;**59**(1):277–82.
56 Soares da Costa TP, Yap MY, Perugini MA, Wallace JC, Abell AD, Wilce MCJ, et al. Dual roles of F 123 in protein homodimerization and inhibitor binding to biotin protein ligase from S taphylococcus aureus. *Mol Microbiol*. 2014;**91**(1):110–20.
57 Soares da Costa TP, Desbois S, Dogovski C, Gorman MA, Ketaren NE, Paxman JJ, et al. Identification of a dimeric KDG aldolase from Agrobacterium tumefaciens. *Proteins*. 2017;**85**(11):2058–65.
58 Soares da Costa TP, Desbois S, Dogovski C, Gorman MA, Ketaren NE, Paxman JJ, et al. Structural determinants defining the allosteric inhibition of an essential antibiotic target. *Structure*. 2016;**24**(8):1282–91.
59 Soares da Costa TP, Christensen JB, Desbois S, Gordon SE, Gupta R, Hogan CJ, et al. Quaternary structure analyses of an essential oligomeric enzyme. *Methods Enzymol*. 2015;**562**:205–23.
60 Laue, T.M., Computer-aided interpretation of analytical sedimentation data for proteins. In: S.E. Harding, J.C. Horton and A.J. Rowe, editors. Analytical ultracentrifugation in biochemistry and polymer science. Cambridge, UK: Royal Society of Chemistry; 1992:90–125.
61 Schuck P, Perugini MA, Gonzales NR, Howlett GJ, Schubert D. Size-distribution analysis of proteins by analytical ultracentrifugation: strategies and application to model systems. *Biophys J*. 2002;**82**(2):1096–111.
62 Schuck P. Size-distribution analysis of macromolecules by sedimentation velocity ultracentrifugation and lamm equation modeling. *Biophys J*. 2000;**78**(3):1606–19.
63 Perugini MA, Schuck P, Howlett GJ. Differences in the binding capacity of human apolipoprotein E3 and E4 to size-fractionated lipid emulsions. *Eur J Biochem*. 2002;**269**(23):5939–49.
64 Maddumage JC, Stewart BZ, Humbert PO, Kvansakul M. Crystallographic studies of PDZ domain-peptide interactions of the scribble polarity module. *Methods Mol Biol*. 2021;**2256**:125–35.
65 Kabsch W. XDS. *Acta Crystallogr D Biol Crystallogr*. 2010;**66**(Pt 2):125–32.
66 Evans P. Scaling and assessment of data quality. *Acta Crystallogr D Biol Crystallogr*. 2006;**62**(Pt 1):72–82.
67 McCoy AJ. Solving structures of protein complexes by molecular replacement with Phaser. *Acta Crystallogr D Biol Crystallogr*. 2007;**63**(Pt 1):32–41.
68 Emsley P, Lohkamp B, Scott WG, Cowtan K. Features and development of Coot. *Acta Crystallogr D Biol Crystallogr*. 2010;**66**(Pt 4):486–501.
69 Meyer PA, Socias S, Key J, Ransey E, Tjon EC, Buschiazzo A, et al. Data publication with the structural biology data grid supports live analysis. *Nat Commun*. 2016;**7**:10882.
70 Pettersen EF, Goddard TD, Huang CC, Couch GS, Greenblatt DM, Meng EC, et al. UCSF Chimera?A visualization system for exploratory research and analysis. *J Comput Chem*. 2004;**25**(13):1605–12.